Morphological investigation of polydisperse asymmetric block copolymer systems of poly(styrene) and poly(methacrylic acid) in the strong segregation regime

Asad Ayoubi, Mehran; Zhu, Kaizheng; Nystrom, Bo; Olsson, Ulf; Almdal, Kristoffer; Khokhlov, Alexei R.; Piculell, Lennart

Published in:
Journal of Polymer Science. Part B, Polymer Physics

Link to article, DOI:
10.1002/polb.23389

Publication date:
2013

Document Version
Publisher's PDF, also known as Version of record

Morphological Investigation of Polydisperse Asymmetric Block Copolymer Systems of Poly(styrene) and Poly(methacrylic acid) in the Strong Segregation Regime

Mehran Asad Ayoubi,[1] Kaizheng Zhu,[2] Bo Nyström,[2] Ulf Olsson,[1] Kristoffer Almdal,[3] Alexei R. Khokhlov,[4] Lennart Piculell[1]

[1]Division of Physical Chemistry, Center for Chemistry and Chemical Engineering, Lund University, SE-22100 Lund, Sweden
[2]Department of Chemistry, University of Oslo, Blindern, N-0315, Oslo, Norway
[3]Department of Micro- and Nanotechnology, Technical University of Denmark, DTU Nanotech, DK-2800 Kongens Lyngby, Denmark
[4]Physics Department, Moscow State University, Moscow 119991, Russian Federation
Correspondence to: M. Asad Ayoubi (E-mail: mehran.asad_ayoubi@fkem1.lu.se)

Received 29 July 2013; revised 19 September 2013; accepted 19 September 2013; published online 9 October 2013
DOI: 10.1002/polb.23389

ABSTRACT: Samples of compositionally (highly) asymmetric diblock copolymers and, also, mixtures of diblock and triblock copolymers (the latter obtained as end-coupling products of two diblock molecules of the mixture), composed of (a) monodisperse majority block(s) of poly(styrene) (PS) and a polydisperse minority block of poly(methacrylic acid) (PMAA), microphase separate into spherical PMAA microdomains, either in disordered liquid-like state or body-centered-cubic (BCC) arrangement, at various annealing temperatures *T*, in the strong segregation regime SSR. We found that (i) the microphase separated state is favored over an anticipated molecularly homogenous state, (ii) the spherical microdomain morphology (with BCC symmetry) is favored over an anticipated hexagonally packed cylindrical morphology, (iii) the extent of the dissolution of short PMAA blocks in the PS material can be quantified, (iv) the spherical microdomains are dilated, and (v) despite molecular-weight (and architectural) polydispersity, well-ordered BCC structures can be obtained. © 2013 Wiley Periodicals, Inc. J. Polym. Sci. Part B: Polym. Phys. **2013**, *51*, 1657–1671

KEYWORDS: block copolymers; block polydispersity; microdomain morphology; microphase separation; SAXS; rheology, self-assembly; WAXS

INTRODUCTION Block copolymers are composed of two or more chemically distinct, and frequently immiscible polymer blocks covalently bound together. For a diblock copolymer (A-B) the interfacial tension between A-block and B-block gives rise to the appearance of A-rich and B-rich microdomains in the melt state. The final morphology of the system is the result of the balance between this enthalpic driving force and entropic costs of (i) localization of the block joints at the interface and (ii) stretching of A and B chains in their domains for maintaining uniform density throughout the system. Conventionally, the enthalpic and entropic contributions are unified in a single parameter χZ, where χ is the Flory-Huggins interaction parameter between the repeat units of A- and B-chains and Z is the total number of segments of the block copolymer. Melt phase diagrams are usually represented in terms of χZ and the volume fraction of one of the blocks. For well-segregated systems the geometry of the microdomains are typically spherical (SPH), cylindrical, (C), or lamellar (L).[1]

Anionic polymerization techniques have been widely used for producing block copolymers and in majority of cases narrow molecular weight distributions have been achieved, with polydispersity indices (PDI = M_w/M_n) close to 1. Consequently, the physics of self-assembly in these materials have traditionally been discussed assuming a narrow molecular weight distribution. However, with recent developments in controlled radical polymerization methods, comprising of atom transfer radical polymerization (ATRP)[2–4] and reversible addition fragmentation transfer[5,6] techniques, the assumption of a narrow molecular weight distribution is no longer necessarily valid. Thus, there is a considerable current interest to reconsider some of the features of self-assembly in light of these synthesis developments, in particular the phase behavior in the melt state.[7]

Additional Supporting Information may be found in the online version of this article.

For a diblock copolymer composed of one monodisperse (MD) A-block and one polydisperse (PD) B-block [i.e., A(MD)-B(PD) system] a number of effects may arise. First, there is a shift in the phase boundaries toward higher volume fractions of B (Φ_B), as observed in experiments[8,9] and predicted by theory.[10,11] The main reason behind this shift is the reduction of the entropic elasticity in the PD domains,[12] facilitating the formation of an interface curved towards them. More specifically, since shorter B-blocks do not extend far from the interface, longer B-blocks can have a less stretched conformation in the space filled further away from the interface, thus decreasing their elastic stretching free energy. Second, there is an increase in B microdomain size D (or periodicity) in comparison to the case where the B-block is monodisperse (D_0).[9,10,12–19] This is also a consequence of decreased entropic elasticity of the B-blocks, simply because for a constant force PD B-blocks can stretch more than their MD counterparts.[10,12,13]

Third, there is a possibility that diblocks with the short B-blocks are dislodged from the interface and swell the domains of the A-blocks.[12] The enthalpic penalty for such a transfer of short B-blocks from the B to the A domains is more than compensated by an increase in the entropy of the system through the delocalization of some junctions points from the interface, as well as the accompanied relaxation of the A-block chains. In principle, this effect induces a reduction of the packing frustrations throughout the system, thus stabilizing ordered morphologies other than body-centered-cubic BCC (e.g., closed-packed structures[11]) or promoting a disordered liquid-like state for the SPH microdomains. A fourth effect of polydispersity on the phase behavior of block copolymers includes a change in segregation strength at the order-disorder transition, $(\chi Z)_{ODT}$. Earlier theoretical studies[10,14,15,20,21] state that polydispersity brings about a general reduction in the values of $(\chi Z)_{ODT}$. For diblock copolymers this phenomenon was only observed experimentally for systems with PD minority blocks.[8,22] By contrast, for diblocks with PD majority blocks, experiments have shown that polydispersity increases values of $(\chi Z)_{ODT}$,[22] in line with more recent simulation studies[23,24] that appear to resolve the discrepancy between earlier theoretical works and the available experimental results. Finally, there is a possibility of macrophase separation.[11] For diblock copolymers, the latter phenomenon has so far only been observed for systems with discrete distributions (diblock copolymer blends)[17] and not for unimodal distributions.

The effects of block polydispersity for systems other than diblocks have also been studied.[25–27] It was shown that for A(PD)-B(MD)-A(PD) and A(MD)-B(PD)-A(MD) systems (i) the morphological boundaries are shifted to higher values of the composition of the PD block,[25,27] and (ii) the L microdomains are dilated.[27] Additionally, it was found that for nearly compositionally symmetric triblock copolymers of the type A(MD)-B(PD)-A(MD), polydispersity increases the microphase separation tendency of the system.[26]

PD block copolymer systems can also be obtained by blending diblocks and triblocks. Previous reports concerning structural properties of such multi-architectural systems are noticeably scarce.[28,29] We believe that understanding microphase separation characteristics of these systems are important, because it is known that even in a well-controlled ATRP synthesis of A-B diblock copolymers a fraction of A-B-A triblock copolymers are produced, as a result of a coupling reaction between two diblock macroradicals.[30]

While there are some previous experimental studies on the effect of polydispersity on phase behavior and microdomain characteristics of symmetric diblock copolymers ($\Phi_B = 0.5$) with L microdomain morphology,[9,17,19] examples of asymmetric cases ($\Phi_B < 0.5$) are limited,[8,9] especially for SPH microdomains.[16] In the only example that we are aware of for SPH microdomains, Nguyen et al.[16] found that polydispersity increased the SPH microdomain size of a number of poly(styrene)-*b*-poly(4-vinylpyridinium methyl iodide) asymmetric diblock copolymers with PD minority ionomeric blocks (up to $PDI_{ionomer} = 3.6$), prepared by blending several block copolymers. They did not find the same behavior for poly(styrene)-*b*-poly(cesium methacrylate) blends. This was attributed to the nonequilibrium nature of the sample preparation techniques that were applied to the acidic block of the parent poly(styrene)-*b*-poly(methacrylic acid) (S-MAA) diblock copolymer for obtaining its cesium-neutralized form. In neither of the cases did they observe macrophase separation. Moreover, in both of the cases, the SPH microdomains lacked liquid-crystalline order, which is in line with the experimental observation that, in block copolymer systems containing PD blocks, the (anticipated) non-lamellar microdomains do not tend to exhibit (well-ordered) liquid-crystalline phases.[8,25,26,31]

It is necessary to point out that while the phenomenon of the dissolution of the short blocks of the PD block in the domain(s) of the MD block has been addressed in many theoretical studies[12,15,24,32] and invoked by a number of experimental works[25,27], to our knowledge, its extent has never been experimentally quantified.

Thus, in this work, for melt self-assembly of compositionally (highly) asymmetric systems of (i) diblock copolymers of the type S(MD)-MAA(PD), and (ii) mixtures of diblock S-MAA and triblock S-MAA-S copolymers where the triblock molecules are the product of a coupling reaction between two diblock macroradicals [in systems of (ii) the poly(styrene) (PS) blocks of the diblocks and triblocks have identical average molecular weights and are MD, whereas the poly(methacrylic acid) (PMAA) blocks have different average molecular weights and are PD], the main points of focus are: (1) to study the effects of block polydispersity on phase behavior and SPH microdomain size characteristics, (2) to quantify the extent of the dissolution of the short blocks of the PD block in the matrix of the MD blocks, and (3) to explore the possibility of obtaining microphase separated SPH microdomains with a high degree of liquid-crystalline order. Furthermore, since it is expected that for compositionally (highly) asymmetric block copolymer systems consisting of majority MD blocks and minority PD blocks there should be a substantial amount of small chains of the minority block that are unanchored from the interface, leave their domains and

TABLE 1 Characteristics of the Neat Diblock Copolymers and the Diblock Fractions of the Mixture M Systems Studied in This Work

Sample	M_n (10^3 g mol^{-1})[a]	PDI_{total}[a]	PDI_{PS}[b]	Z_{PS}[c]	Z_{PMAA}[d]	Φ_{PMAA}[e]
S(MD)-MAA(PD)-3[f]	47.2	1.07	1.07	440	17[g]	0.03
S(MD)-MAA(PD)-8-M[h]	–	–	1.10	155	18[i]	0.08
S(MD)-MAA(PD)-15[f]	39.8	1.10	1.05	318	78[g]	0.15
S(MD)-MAA(PD)-17-M[h]	–	–	1.10	155	43[i]	0.17
S(MD)-MAA(PD)-30-M[h]	–	–	1.10	155	91[i]	0.30

[a] Calculated from SEC of S-tBMA for S-MAA.
[b] From SEC.
[c] Z_{PS} stands for number average degree of polymerization of PS-block and is calculated from SEC analysis.
[d] Z_{PMAA} stands for number average degree of polymerization of PMAA-block.
[e] $\Phi_{PMAA}=Z_{PMAA}v_{PMAA}/(Z_{PMAA}v_{PMAA}+Z_{PS}v_{PS})$, where the segmental monomer volumes of v_{PMAA} =117 Å^3 and v_{PS} =165 Å^3 are calculated from the density and the segmental molar mass values of ρ_{PMAA} = 1.22 g cm^{-3},[33] ρ_{PS} = 1.05 g cm^{-3},[34] M_{MAA} = 86 and M_S = 104.
[f] Neat diblock copolymer system.
[g] Calculated using values of mass composition (obtained from ^{1}H NMR) and Z_{PS}.
[h] Diblock/triblock mixture M system (see the Supporting Information 1).
[i] Calculated using values of mass composition of the mixture system (obtained from ^{1}H NMR) and Z_{PS} assuming that in the mixture system fractions of the diblocks and the triblocks have the same compositions (see subsection Characterization).

enter into and swell the majority block domain(s), it is essential to chose systems that are in the strong segregation regime SSR, thus limiting the extent of the dissolution of the short PD blocks in a physically tractable manner. For systems studied in this work a high thermodynamic incompatibility between PS and PMAA, reflected in their solubility parameters[34] (δ_{PS} = 22.69 vs. δ_{PMAA} = 26.80 MPa$^{1/2}$), and the molecular weights chosen (see Table 1 and subsection "Characterization") ensure this possibility.

We have interpreted our experimental results obtained for the diblock systems and the mixed diblock/triblock systems by comparing them with the predicted microphase separation behavior of the MD equivalent systems of diblocks and triblocks. For identifying the characteristics of these MD equivalent systems we have used the self-consistent-field-theory SCFT of Helfand and Wassermann[35–38] (HW) for prediction of the phase diagrams of diblock and triblock copolymers, and the SSR theories by Nyrkova et al.[39] (NKD) and Semenov et al.[40] (SNK) for prediction of SPH microdomain sizes of diblock copolymers.

The Results and Discussion part of the paper is organized as follows. Block copolymer SPH microdomains in the disordered liquid-like state at low Φ_{PMAA} values are analyzed in subsection "SPH microdomains in disordered liquidlike state at low Φ_{PMAA}." SPH microdomains in ordered liquid-crystalline states appearing at higher Φ_{PMAA} values are considered in subsection "SPH microdomains in ordered liquid crystalline state at high Φ_{PMAA}." Effects of polydispersity on the phase behavior and the size characteristics of our system are discussed in subsection "Effect of polydispersity on the microphase separation behavior."

EXPERIMENTAL

Materials

Five different block copolymer systems of PS and PMAA are used in this study, including two systems of diblocks [symbolized as S(MD)-MAA(PD)-3 and S(MD)-MAA(PD)-15] and three mixture M systems containing diblocks and triblocks [symbolized as S(MD)-MAA(PD)-8-M, S(MD)-MAA(PD)-17-M and S(MD)-MAA(PD)-30-M] (see Table 1; the number in the sample codes indicates the volume percentage of PMAA block%$_{PMAA}$; %$_{PMAA}$ = 100 × Φ_{PMAA}).

Two diblock copolymer samples of S(MD)-MAA(PD)-3 and S(MD)-MAA(PD)-15 (Table 1) were purchased from Polymer Source. They were synthesized through anionic polymerization[41] and the molecular weight was characterized by size exclusion chromatography (SEC) and ^{1}H NMR. The corresponding characterization by Polymer Source is reproduced in Table 1.

The other three block copolymer systems prepared for this study [i.e., S(MD)-MAA(PD)-8-M, S(MD)-MAA(PD)-17-M, and S(MD)-MAA(PD)-30-M] were synthesized via a modified "three-step" procedure comprising of two steps of ATRP and one hydrolysis reaction (Fig. 1).[42,43] The synthetic methodology that we have adopted is a "classic" ATRP method, although recently improved versions of it have also appeared.[44] All the chemicals used for the latter synthesis were purchased from Aldrich. Styrene (St) and *tert*-butyl methacrylate (*t*-BMA) were distilled in high vacuum, degassed, and stored in a brown glass bottle at 18 °C before usage. 1-Bromoethyl benzene (1-BrEB) and *N*, *N*, *N*′,*N*″,*N*″-pentamethyldiethylenetriamine (PMDETA) were distilled under vacuum and stored in a brown glass at 5 °C. Copper (I) bromide was purified by washing with glacial acetic acid, followed by absolute ethanol and ethyl ether. Then they were dried under vacuum and kept under argon atmosphere.

Synthesis

Procedure for the ATRP Synthesis of Polystyrene-Macroinitiatior (PS-MI)

Polymerization of styrene was carried out via an ATRP procedure. CuBr (430 mg, 3 mmol) was added to a round-bottom flask. The flask was sealed with a rubber septum, evacuated and backfilled three times with argon, and then left

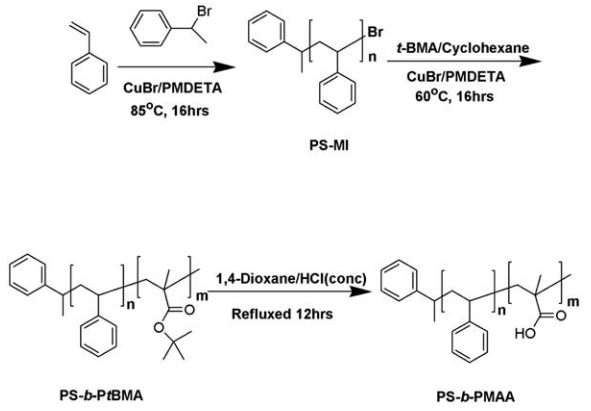

FIGURE 1 Schematic illustration of the synthesis of S-MAA block copolymer via ATRP.

under argon. In the next step, styrene (103 mL, 0.9 mol) was added to the flask and was further degassed with three freeze-pump-thaw cycles. Deoxygenated PMDETA (0.63 mL, 3 mmol) was added via a syringe. The solution turned light green as complex formation occurred and remained heterogeneous. After the majority of the metal complex had formed, 1-BrEB (0.42 mL, 3 mmol) was added via a syringe. The reactor was then placed in an oil bath, which was previously preheated to 85 °C. The reaction mixture progressively became green and more viscous. After 16 h, the reactor was removed from the oil bath and allowed to cool down to room temperature. A small amount of sample was withdrawn and dissolved into $CDCl_3$ for determination of degree of conversion of the monomer. The mixture was diluted with 100 mL THF and passed through Al_2O_3 (basic, activated) column to remove the copper catalyst. The mixture was concentrated and precipitated into CH_3OH. The precipitation procedure was repeated several times until the polymer precipitated as a powder instead of a sticky liquid. It was then dried under vacuum (at 70 °C, at least for 24 h) and analyzed by ^{1}H NMR and SEC to determine the degree of polymerization (Z_{PS} = 155, M_n = 16300, PDI_{PS} = 1.10; see Table 1). It was used as the initiator to conduct the next step of the ATRP synthesis of the block copolymer systems of S-*t*BMA-M.

Procedure for the ATRP Synthesis of Block Copolymer Systems of S-tBMA-M

The synthesis procedure is very similar to the synthesis of PS-MI mentioned above, except that the PS-MI and CuBr were added to the flask initially and cyclohexane was used as the solvent and the polymerization was kept at 60 °C for several hours. The final white product was collected by precipitation into CH_3OH/H_2O (v/v = 1/1) and dried in vacuum at 40 °C for 24 h. The chosen monomer/macroinitiator (*t*-BMA/PS-MI) molar ratios were 24/1, 60/1, and 120/1. The values of the weight fractions of P*t*BMA block in the resultant block copolymer systems w_{PtBMA} were calculated from the integral values of the ^{1}H NMR spectra of the characteristic peak of $(CH_3)_3C$— (δ = 1.4 ppm) of *t*-BMA, the typical peak of the phenyl (δ = 6.5 − 7.0 ppm) of styrene and the known number of repeat units of styrene (Z_{PS} = 155), which equal w_{PtBMA} = 0.14, 0.28, and 0.45.

Procedure for Hydrolysis Synthesis of Block Copolymer Systems of S-MAA-M

First, the block copolymers synthesized in the previous steps were dissolved in equal amounts of dioxane by weight. Then, based on the number of moles of ester groups present in the block copolymer/dioxane solutions, concentrated HCl in threefold excess was added. The mixture was heated to reflux for ~12 h. The polymers were then precipitated into water, washed with water several times, and dried under vacuum. ^{1}H NMR analysis in 1,4-dioxane-d_8 showed the disappearance of the *tert*-butyl resonance at δ = 1,4 ppm indicating the success of the cleavage reaction of the *tert*-butyl group from the polymer chain. Thus, S(MD)-MAA(PD)-8-M, S(MD)-MAA(PD)-17-M, and S(MD)-MAA(PD)-30-M samples were obtained.

Characterization

For an A-B diblock copolymer, when formation of the blocks are statistically independent from each other it is possible to relate individual polydispersity indices of A- and B-blocks (PDI_A and PDI_B, respectively) to that of the diblock copolymer (PDI_{A-B}) through their weight fractions (w_A and w_B). The corresponding expression relating these parameters was derived for Schultz-Zimm distribution of the chain lengths,[45] as well as the general case of the chain length distribution function[7] in the following manner:

$$PDI_{A-B} = w_A^2(PDI_A - 1) + w_B^2(PDI_B - 1) + 1 \quad (1)$$

Usually PDIs of the diblock copolymer PDI_{A-B} and one of the blocks (e.g., PDI_A) are known and one can calculate PDI_B. For a highly asymmetric diblock copolymer ($\Phi_B < 0.3$) the thus calculated value for PDI_B has a large uncertainty. For diblock copolymers of S(MD)-MAA(PD)-3 and S(MD)-MAA(PD)-15, from the known values of PDI_{total} and PDI_{PS} (see Table 1), we obtained values of PDI_{PMAA} of about 3. Although this value is uncertain, it is sufficiently high to clearly demonstrate the PD nature of the PMAA block, which is what concerns us in this study.

For polymers synthesized in this study, SEC was performed at room temperature with two mixed-D columns from Polymer Laboratories. THF was used as the mobile phase and the flow rate was 0.5 mL min^{-1}. For S-MAA, it was not possible to find a common single solvent, so for the chromatography we used the nonhydrolyzed S-*t*BMA, which is soluble in THF. As shown in the Supporting Information 1, the chromatograms revealed bimodal distributions for the copolymers, featuring in addition to the diblock fraction an additional high-molecular weight fraction that was absent for the macroinitiator. The detailed analysis showed that the high-molecular weight fraction had a degree of polymerization that, to a very good approximation, corresponded to twice that of the diblock fraction. Thus, the additional fraction could be identified as triblocks resulting from a coupling reaction between two diblock macroradicals. The mass fraction of triblocks in the mixture, as obtained from simulations

of the SEC chromatograms, was found to be of the order 0.2–0.6 (see Supporting Information 1), increasing with an increasing length of the PMAA block. Owing to the complex nature of the chromatograms for the mixtures, we regard the molecular weights of the individual diblocks and triblocks obtained from the simulations of the chromatograms to be quantitatively unreliable. For S(MD)-MAA(P)-8-M, S(MD)-MAA(PD)-17-M, and S(MD)-MAA(PD)-30-M, we therefore instead used the values of Z_{PS} (=155), obtained from SEC of the macroinitiator, together with the values Φ_{PMAA} (=0.08, 0.17, and 0.30), obtained from the ^{1}H NMR analysis of the copolymers (subsection "Procedure for the ATRP synthesis of block copolymer systems of S-tBMA-M"), to calculate the values of Z_{PMAA} for the diblocks and triblocks. The latter values varied in the range $18 \leq Z_{PMAA} \leq 182$.

Sample Preparation

The samples were annealed at different temperatures under high vacuum or nitrogen atmosphere for various time periods followed by subsequent rapid quenching in dry ice or water. There is a possibility of anhydride formation of PMAA block at elevated temperature[46] accompanied by color change in the block copolymer. A significant color change was indeed observed for trial samples treated for very long times at high temperatures. However, no such samples were used in our analysis.

Shear alignment of samples was carried out using a home-built shearing device. The shearing device is made of two aluminum plates (one stationary and another moving) each equipped with temperature control units (± 0.1 °C). The plates can be cooled down rapidly by flushing water through interior channels. The frequency, the strain amplitude and the distance between the plates can be adjusted and the movement of the moving plate relative to the stationary one is sinusoidal. Typically, a frequency of 6 rpm, strain amplitude of 500% and a thickness of 1 mm were chosen. To avoid degradation, the whole instrument was put in a chamber purged with nitrogen.

Throughout this article, the reported value for temperature T is the temperature at which annealing or shear alignment was performed. High glass transition temperatures of PS[34] (T_g^{PS} = 100 °C) and PMAA[46] (T_g^{PMAA} = 129 − 170 °C) ensure retainment at ambient temperature of the structure formed at an elevated temperature.

X-ray Scattering

Small- and wide-angle X-ray scattering (SAXS and WAXS) were performed at beamline I711 at the MaxLab synchrotron facility in Lund, Sweden. The intensity $I(q)$ was measured at room temperature as a function of the scattering vector q (= $(4\pi/\lambda)$ sin θ, where 2θ is the scattering angle and the wavelength of the X-ray beam was λ = 1.1 Å).

Rheology

Rheological measurements were conducted using a Physica MCR102 rheometer (Anton Paar). A plate-plate geometry was used. The shear storage modulus (G') was measured during an isochronal heating temperature ramp (1 °C min^{-1}) with 1% strain amplitude and a frequency of ω = 1 rad s^{-1}. The low strain amplitude chosen ensures that the rheological measurement is performed in the linear viscoelastic regime.

RESULTS AND DISCUSSION

SPH Microdomains in Disordered Liquid-Like State at Low Φ_{PMAA}

First, we consider morphologies of systems with the lowest Φ_{PMAA} values: the block copolymer systems of S(MD)-

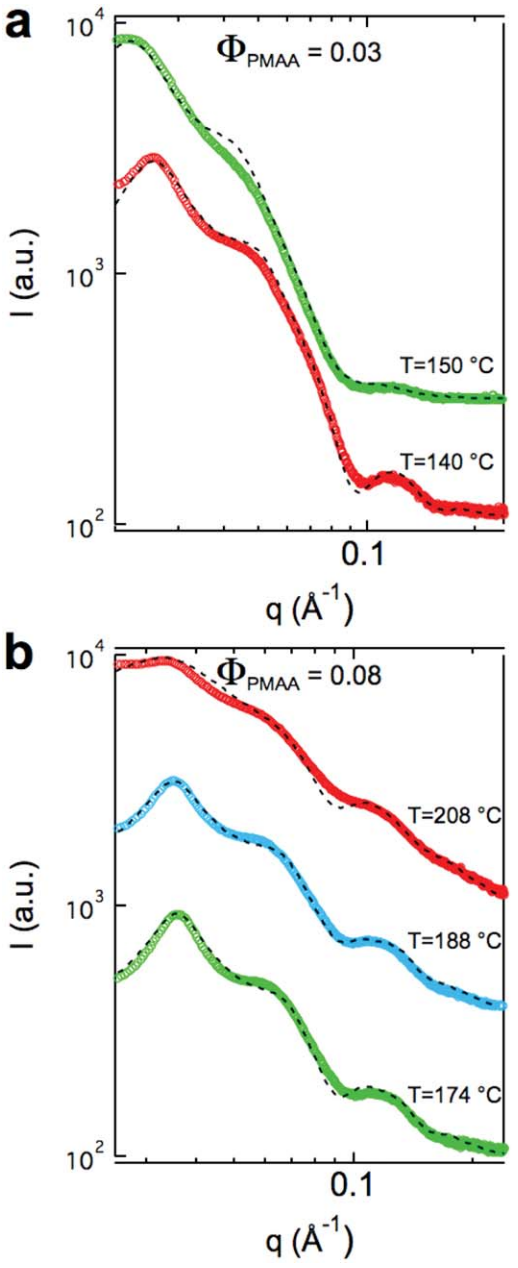

FIGURE 2 SAXS results for (a) S(MD)-MAA(PD)-3 at T = 140°C (red) and 150°C (green), and (b) S(MD)-MAA(PD)-8-M at T = 174°C (green), 188°C (blue), and 208°C (red). In (a) and (b) dashed black lines through the data are the simulated intensities of the proposed model for the SPH microdomains (eqs 2–6).

TABLE 2 SAXS Modeling Parameters and SPH Microdomain Characteristics for Disordered Liquid-like State for S(MD)-MAA(PD)-3 and S(MD)-MAA(PD)-8-M Systems

	Φ_{PMAA}	T (°C)	$R_{ex,P(q)}$ (Å)[a]	Φ_{hs} (±0.05)[a,b]	R_{hs} (±5 Å)[a,b]	σ (Å)[a]	s[a]
S(MD)-MAA(PD)-3	0.03	140	47	0.30	122	5	0.10
		150	45	0.24	137	9	0.19
S(MD)-MAA(PD)-8-M	0.08	174	47	0.41	92	6	0.13
		188	46	0.41	94	6	0.14
		208	48	0.25	98	7	0.15

[a] From modeling.
[b] The stated value for the uncertainty interval of a given parameter was determined through visual inspections of the simulated scattering patterns when the parameter in question was changed and all the other ones were kept unchanged, and should be considered as a rough estimate that captures the upper-limits of the allowed deviations from the reported value of the parameter.

MAA(PD)-3 ($\Phi_{PMAA}=0.03$) and S(MD)-MAA(PD)-8-M ($\Phi_{PMAA}= 0.08$). SAXS results for different annealing temperatures are presented in Figure 2. The scattering patterns lack any Bragg peak representative of long-range order. However, they show oscillations at high and low-q. The former is attributed to single particle scattering [form factor $P(q)$] and the latter to interference from their spatial arrangement [structure factor $S(q)$]. For a detailed interpretation of scattering patterns we utilized an approach previously adopted for disordered SPH microdomains in block copolymer melts.[47–50] The intensity is related to $P(q)$ and $S(q)$ in the following manner:

$$I(q) \sim P(q)S(q) \tag{2}$$

$P(q)$ for a system of spheres (radius R) is

$$P(q,R)=\left(\frac{4}{3}\pi R^3\right)^2\left(\frac{3[\sin(qR)-qR\cos(qR)]}{(qR)^3}\right)^2 \tag{3}$$

To account for polydispersity in size of spheres we convolute $P(q,R)$ with a Gaussian function $p(R)$ with a standard deviation of σ.

$$P\left(q,\overline{R},\sigma\right)=\frac{\int_0^\infty P(q,R)p(R)dR}{\int_0^\infty p(R)dR} \tag{4}$$

$$p(R)=\mathrm{A}\exp\left[\frac{-(R-\overline{R})^2}{2\sigma^2}\right] \tag{5}$$

Thus, $\overline{R}$ is the average radius of the spheres. For $S(q)$, we have assumed a hard-sphere Percus-Yevick potential between the SPH microdomains for the sake of simplicity. It is based on the Ornstein-Zernike formulation of the total correlation function of particles in terms of direct pair correlation and indirect correlation.[51] Percus and Yevick calculated analytically this total correlation function for a short-range hard-sphere potential between the particles.[52] The final expression for $S(q)$ for an effective hard sphere radius R_{hs} and an effective hard sphere volume fraction Φ_{hs} reads as[53,54]

$$\begin{aligned}
&S(q,R_{hs},\Phi_{hs})=\frac{1}{1+24\Phi_{hs}\left(\frac{G(A)}{A}\right)}\\
&G(A)=\frac{\alpha}{A^2}(\sin A-A\cos A)+\frac{\beta}{A^3}\left(2A\sin A+(2-A^2)\cos A-2\right)\\
&\quad+\frac{\gamma}{A^5}\left(-A^4\cos A+4[(3A^2-6)\cos A+(A^3-6A)\sin A+6]\right)\\
&\alpha=\frac{(1+2\Phi_{hs})^2}{(1-\Phi_{hs})^4},\quad \beta=-6\Phi_{hs}\frac{\left(1+\frac{\Phi_{hs}}{2}\right)^2}{(1-\Phi_{hs})^4},\quad \gamma=\frac{\Phi_{hs}(1+2\Phi_{hs})^2}{2(1-\Phi_{hs})^4},\\
&A=2qR_{hs}
\end{aligned} \tag{6}$$

The scattering intensity of the above mentioned model is compared with scattering curves of S(MD)-MAA(PD)-3 and S(MD)-MAA(PD)-8-M. Very good agreement between the model and the experimental data (Fig. 2) is obtained. The extracted values for the average radius of the SPH microdomains $R_{ex,P(q)}$ ($=\overline{R}$ in eqs 4 and 5), R_{hs}, Φ_{hs}, σ, and the relative standard deviation of the radius s ($=\frac{\sigma}{R_{ex,P(q)}}$) are presented in Table 2.

For S(MD)-MAA(PD)-3, an increase in temperature from 140 to 150 °C essentially does not change $R_{ex,P(q)}$ values of the SPH microdomains, but effectively increases their size polydispersity[55] reflected in σ (σ = 5 and 9 Å for T = 140 and 150 °C, respectively). For samples with S(MD)-MAA(PD)-8-M the same scenario is valid for $R_{ex,P(q)}$ but the degree of polydispersity in size ($\sigma \approx 6$ Å) does not change significantly with temperature.

When the PD nature of the PMAA block is coupled with a short length, there is a possibility that a fraction of very short PMAA blocks $\Delta\Phi_{PMAA}$ are dislodged from the PMAA domains to enter into, and swell the PS matrix, despite the high degree of thermodynamic incompatibility between the two blocks. The modeling approach that we have adopted allows us to determine (i) the volume fraction of the PMAA chains that are segregated into the SPH microdomains Φ^{Seg}_{PMAA}, and thus the value of $\Delta\Phi_{PMAA}$ in the following manner,

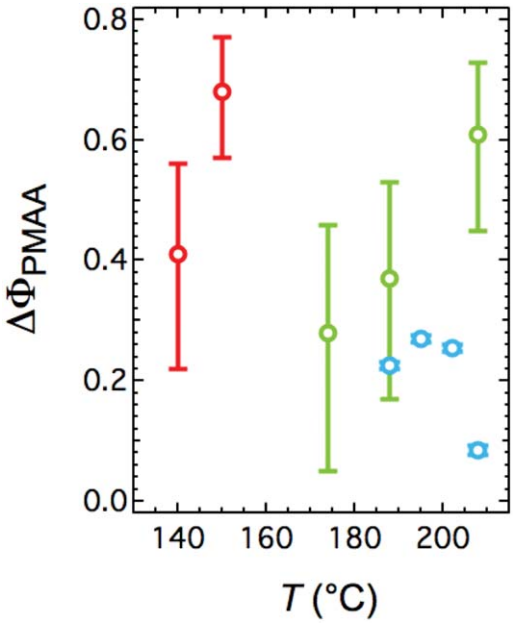

FIGURE 3 Values of the fraction of the short PMAA blocks $\Delta\Phi_{PMAA}$ that are dislodged from the interface and enter into, and swell the PS matrix are shown for different annealing temperatures T for S(MD)-MAA(PD)-3 (red; using eq 7), S(MD)-MAA(PD)-8-M (green; using eq 7), and S(MD)-MAA(PD)-17-M (blue; using eq 11). The error bars for each data point were calculated using the uncertainty intervals of the input parameters of the used equation.

$$\Delta\Phi_{PMAA}=1-\frac{\Phi_{PMAA}^{Seg}}{\Phi_{PMAA}}=1-\frac{\Phi_{hs}\int_0^{\infty}(R/R_{hs})^3p(R)dR}{\Phi_{PMAA}\int_0^{\infty}p(R)dR} \quad (7)$$

$p(R)$ being defined in eq 5 with $\overline{R}=R_{ex,P(q)}$, and (ii) the average radius of the SPH microdomains $R_{ex,P(q)}$ without any assumption regarding $\Delta\Phi_{PMAA}$. It is necessary to highlight three facts here: (i) the SPH microdomains have a low degree of polydispersity in size, (ii) the size of the SPH microdomains in liquid-like state is independent of the annealing temperature T, and (iii) $\Delta\Phi_{PMAA}$ has nonzero values that increases upon an increase in T (see Fig. 3). For block copolymer systems consisting of MD and PD blocks, to our knowledge, this is the first time that the extent of the dissolution of the short blocks of the PD block in the matrix of the MD block is quantified. Moreover, a Monte Carlo study for an A(MD)-B(PD) system ($\Phi_B < 0.5$) predicts that $\Delta\Phi_B$ should increase when the temperature increases,[24] which is in line with our findings for S(MD)-MAA(PD)-3 system. (Further interpretations of the results of this analysis are presented in subsections "S(MD)-MAA(PD)-%PMAA Diblock Systems" and "S(MD)-MAA(PD)-%PMAA-M Diblock/Triblock Mixture Systems").

Thus, S(MD)-MAA(PD)-3 and S(MD)-MAA(PD)-8-M systems predominantly consist of nearly MD in size PMAA-filled spherical SPH(PMAA) microdomains dispersed in a matrix of PS chains in a disordered liquid-like state.

SPH Microdomains in Ordered Liquid-Crystalline State at High Φ_{PMAA}

Rheology

In an attempt to locate any ODT we performed isochronal temperature sweep measurements of G' for S(MD)-MAA(PD)-15, S(MD)-MAA(PD)-17-M, and S(MD)-MAA(PD)-30-M systems. The results are shown in Figure 4. For S(MD)-MAA(PD)-15, G' decreased steadily with an increase in temperature and underwent a moderate drop at about 200 °C. For S(MD)-MAA(PD)-17-M and S(MD)-MAA(PD)-30-M systems these drops were more pronounced and occurred at about 195 and 185 °C, respectively. We cannot attribute these sudden changes to ODT, as the terminal values of G' are still high (several hundred Pa), far from the low values expected for the disordered state. This is supported by the SAXS result of S(MD)-MAA(PD)-17-M at T = 208 °C that shows a BCC structure (see below subsection "SAXS" and Fig. 5). Possibly, this change is due to a transition from a glassy state into a rubbery state expected to occur in the vicinity of the glass transition temperature of the PMAA block.[46] Thus, we may conclude that up to 230 °C no ODT is observed for S(MD)-MAA(PD)-15, S(MD)-MAA(PD)-17-M, and S(MD)-MAA(PD)-30-M systems.

SAXS

S(MD)-MAA(PD)-15 System

Scattering intensities of the system of S(MD)-MAA(PD)-15 at T = 188 and 202 °C are presented in Figure 5(a). At T = 202 °C the peak with the maximum intensity q^* is located at 0.0176 Å^{-1} and there is a distinct peak at $\sqrt{2}q^*$ (=0.0249 Å^{-1}) and two possible peaks at $\sqrt{4}q^*$ (=0.0353 Å^{-1}) and $\sqrt{5}q^*$ (=0.0394 Å^{-1}), which are not very well resolved. There is also a broad peak centered at 0.0636 Å^{-1}. Shear alignment

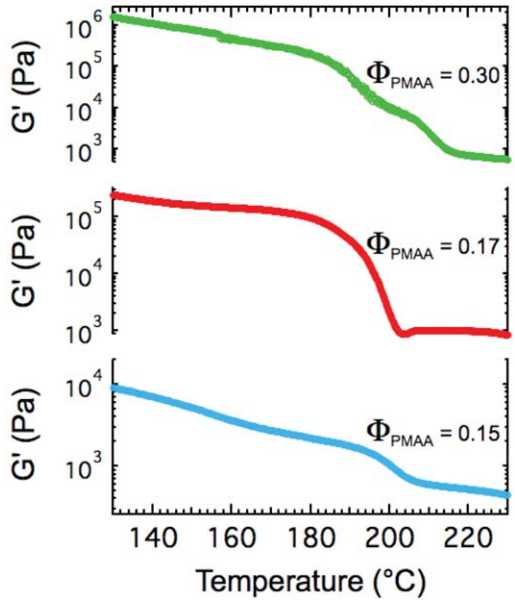

FIGURE 4 Isochronal temperature sweep measurements of G' for the systems of S(MD)-MAA(PD)-15 (blue), S(MD)-MAA(PD)-17-M (red), and S(MD)-MAA(PD)-30-M (green) measured at 1% strain amplitude and a frequency of ω = 1 rad s^{-1}.

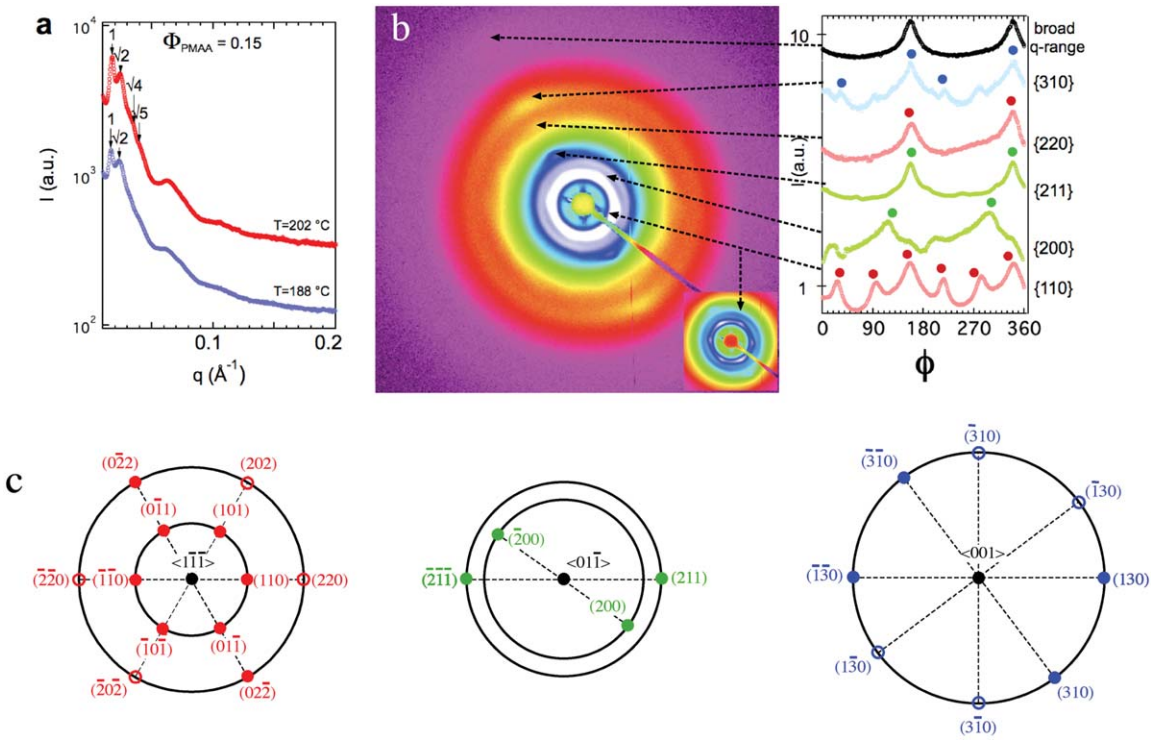

FIGURE 5 (a) Powder SAXS results for the system of S(MD)-MAA(PD)-15 at T = 188°C (blue) and T = 202°C (red). Observed positions of BCC reflections are indicated. (b) 2-D SAXS result for sheared system of S(MD)-MAA(PD)-15 at T = 202°C, together with azimuthal intensity for observed BCC reflections. (c) Predicted diffraction patterns for a BCC crystal when the beam is incident along the directions of $\langle 1\bar{1}\bar{1}\rangle$ (left), $\langle 01\bar{1}\rangle$ (middle) and $\langle 001\rangle$ (right); the full (b and c) and the hollow (c) circles indicate the present and the absent reflections in our experiments, respectively.

of the block copolymer samples has proved to be a valuable tool for increasing the grain size and alignment of the domains, which results in better resolution in scattering patterns.[1] We have applied this technique for this sample and the results are shown in Figure 5(b). In the scattering pattern, moving away from the beam center, it is observed that, (i) the q-vector location of the first and second sets of diffraction spots are similar to those of the q^* and $\sqrt{2}q^*$ peaks of powder pattern, (ii) the diffraction spots at $\sqrt{4}q^*$ and $\sqrt{5}q^*$ q-vector positions are now well-resolved, and (iii) new diffraction spots at $\sqrt{3}q^*$ (=0.0305 Å^{-1}) position have appeared. The observed q-vector relative positions (1, $\sqrt{2}$, $\sqrt{3}$, $\sqrt{4}$, and $\sqrt{5}$) provide evidence for the existence of BCC structure. A melt of a block copolymer sample consisting of the SPH microdomains with a powder-like BCC arrangement may respond to shear through changes in the arrangement and the shape of the microdomains.[56–58] In terms of the arrangement, it is often observed that the unit cell is oriented in two different directions[56] (i.e., twinned BCC structure). In terms of the shape, the SPH microdomains can be transformed into the C ones.[57,58] Shear treatment of our sample has resulted in a crystalline structure, but apparently, it is not single domain or twinned, deduced from the following implications. In spite of the fact that the family of {211}-planes is not parallel to the family of {110}- and {220}-planes, its diffraction spots occur at similar azimuthal angles of about ϕ = 157° and 339°. This means that there are at least two orientations for the unit cell of the prepared diblock copolymer crystal, giving rise to such a situation. The same scenario is valid for the diffraction spots of the family of {310}-planes, when compared to those of the family of {110}- and {220}-planes or {211}-planes. Therefore, there are at least three orientations for the BCC unit cell of this diblock copolymer crystal sample. We have compared our experimental azimuthally dependent intensity patterns [Fig. 5(b)] with the diffraction spots of a BCC crystal when the beam is incident along the directions of $\langle 1\bar{1}\bar{1}\rangle$, $\langle 01\bar{1}\rangle$, and $\langle 001\rangle$ [Fig. 5(c)]. Good agreement is obtained between the theoretical and experimental diffraction patterns. Thus, the BCC nature of the morphology of S(MD)-MAA(PD)-15 at T = 202 °C is confirmed.

At T = 188 °C, the nonsheared scattering pattern [Fig. 5(a)] is very similar to the powder SAXS pattern at T = 202 °C and we suggest the existence of BCC morphology at this temperature. The fact that this sample has BCC morphology at these two T values is consistent with the rheology data (Fig. 4) showing that at these temperatures the system is not in a disordered state.

S(MD)-MAA(PD)-17-M System

SAXS patterns for the mixture system of S(MD)-MAA(PD)-17-M annealed at different temperatures T are presented in Figure 6. In all of the scattering patterns, there is a weak peak

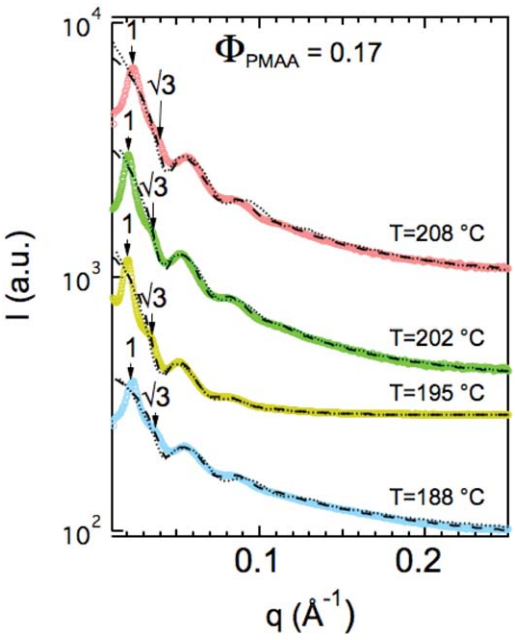

FIGURE 6 SAXS results for the mixture system of S(MD)-MAA(PD)-17-M at T = 208°C (red), T = 202°C (green), T = 195°C (yellow), and T = 188°C (blue). The first two reflections of BCC are specified. The dashed and the dotted lines are the results of simulation to the sphere and cylinder form factors, respectively (see Table 3 for the simulation parameters). The samples were not birefringent when viewed between crossed polarizers.

at $\sqrt{3}q^*$ position, together with intensity oscillations at higher range of the q-vector. The absence of a large number of Bragg reflections makes direct and straightforward SAXS structural analysis a challenging task. In such situations, a common strategy of analysis is to assume various *a priori* morphologies and choose the most relevant one based on space-filling (stoichiometric) and SAXS modeling analyses of the available experimental data.[60,61] We thus start by assuming either SPH or *C* shapes for the microdomains arranged on BCC lattice or in a hexagonal arrangement (i.e., *C*(PMAA) morphology), respectively.

From space-filling geometrical considerations the radii of the SPH microdomains $R_{ex,BCC}$ (for the assumed BCC lattice) and the *C* ones $R'_{ex,C(PMAA)}$ (for the assumed hexagonal lattice) are the following

$$R_{ex,BCC} = \left(\frac{3\Phi_{PMAA}^{Seg}\alpha^3}{4\pi n_u}\right)^{\frac{1}{3}} \quad (8)$$

$$R'_{ex,C(PMAA)} = \left(\frac{\sqrt{3}}{2\pi}\Phi_{PMAA}^{Seg}\alpha'^2\right)^{\frac{1}{2}} \quad (9)$$

where n_u is the number of the spheres in the cubic unit cell (for BCC lattice n_u = 2), and α and α' are the unit cell dimensions of the BCC and 2D-hexagonal lattices, respectively. For the time being, we assume that all of the PMAA blocks are segregated into their respective microdomains and none of them are dissolved in the PS microdomains, that is, $\Phi_{PMAA}^{Seg} = \Phi_{PMAA}$. Thus, the extracted values of $R_{ex,BCC}$ and $R'_{ex,Hex}$ are considered as the upper limit for the size of the SPH and *C* microdomains, respectively. The calculated values for $R_{ex,BCC}$ and $R'_{ex,C(PMAA)}$ are presented in Table 3. (Nevertheless, we will further see that once the morphology is determined, this assumption can be removed and we are also able to determine the value of $\Delta\Phi_{PMAA}$).

In Figure 6, the intensity oscillations at about q = 0.04 − 0.14 Å^{-1} presumably originate from the single-particle (form factor) scattering of the SPH or *C* microdomains. For SPH microdomains, the simulated intensity of a system of PD spheres (eqs 3–5) is used for reproducing the relevant part of the scattering patterns. Very good agreement between the simulated and experimental scattering patterns are obtained (Fig. 6) and the extracted values of the average radius $R_{ex,P(q)}$, its standard deviation σ and the corresponding relative standard deviation s acquired through this analysis for the assumed SPH microdomains are presented in Table 3.

For *C* microdomains the form factor of a cylinder $P'(q)$ should be used, which is given by[62]

$$P'(q,R',L') = \int_0^{\frac{\pi}{2}} f^2(q,\beta)\sin\beta d\beta$$
$$f(q,\beta) = 8\pi R'^2 L' j_0\left(\frac{qL'}{2}\beta\right)\frac{j_1(qR'\sin\beta)}{qR'\sin\beta} \quad (10)$$

where $j_0(x) = \sin x/x$, $j_1(x)$ is the first order Bessel function, R' is the radius of the cylinder, L' is its length, and β is the angle between the cylinder axis and the q-vector. Thus, in eq 10 the cylinder form factor is an average over all possible orientations of the cylinder with respect to the q-vector. We have used Irena SAXS analysis package[59] that has implemented the code for $P'(q)$, convoluted with a Gaussian distribution for R' with a standard deviation of σ'. Very good agreement between the simulated and the experimental scattering patterns are obtained (Fig. 6) and the extracted values of the average radius $R'_{ex,P'(q)}$, its standard deviation σ' and the corresponding relative standard deviation s' ($=\frac{\sigma'}{R'_{ex,P'(q)}}$) acquired through this analysis for the assumed *C* microdomains are presented in Table 3. It should be mentioned that 2D-hexagonal arrangement of the *C* microdomains requires cylinders with $L' >> R'$. In our simulations, for the sake of convenience, we have assumed that $L' = 10R'$; nevertheless, the simulated intensity tend to show little changes when L' values higher than $10R'$ were chosen.

For the assumed BCC forming SPH microdomains, the value (range) of $R_{ex,BCC}$, $R_{ex,P(q)}$, σ, and s are 104 Å $\leq R_{ex,BCC} \leq$ 112 Å, 101 Å $\leq R_{ex,P(q)} \leq$ 108 Å, 10 Å $\leq \sigma \leq$ 11 Å, and s = 0.10, respectively, for various T values. For the assumed 2D-hexagonally arranged *C* microdomains the parameter space window of $R'_{ex,C(PMAA)}$, $R'_{ex,P'(q)}$, σ', and s' are 68 Å $\leq R'_{ex,C(PMAA)} \leq$ 79 Å, 90 Å $\leq R'_{ex,P'(q)} \leq$ 97 Å, 8 Å $\leq \sigma' \leq$ 10 Å, and 0.09 $\leq s' \leq$ 0.11, respectively, for various T values.

TABLE 3 SAXS Modeling Parameters for SPH(PMAA) Microdomains with BCC Arrangement (Together with SPH Microdomain Characteristics) and *C*(PMAA) Morphology, for the Mixture System of S(MD)-MAA(PD)-17-M

	SPH(PMAA) (with BCC arrangement)						C(PMAA)			
T (°C)	α (±1 Å)	$R_{ex,BCC}$[a] (Å)	$R_{ex,P(q)}$[b] (Å)	σ[b] (Å)	s[c]	α' (Å)	$R'_{ex,C(PMAA)}$[d] (Å)	$R'_{ex,P'(q)}$[e] (Å)	σ'[e]	s'[f]
188	415	112	103	10	0.10	339	73	90	8	0.09
195	444	120	108	11	0.10	363	79	97	10	0.10
202	433	117	106	11	0.10	354	77	95	10	0.11
208	385	104	101	10	0.10	314	68	90	8	0.08

[a] From eq 8.
[b] Extracted from simulations (eqs 2–5).
[c] $s=\frac{\sigma}{R_{ex,P(q)}}$
[d] From eq 9.
[e] Extracted from simulations (based on eq 10) by using Irena SAXS analysis package.[59]
[f] $s'=\frac{\sigma'}{R'_{ex,P'(q)}}$.

Comparison of the pairs of $R_{ex,BCC}/R_{ex,P(q)}$ and $R'_{ex,C(PMAA)}/R'_{ex,P'(q)}$ for all of the samples reveals that $R_{ex,BCC} > R_{ex,P(q)}$, and $R'_{ex,C(PMAA)} < R'_{ex,P'(q)}$ (Table 3). As it was mentioned before $R_{ex,BCC}$ and $R'_{ex,C(PMAA)}$ are the upper limits for the size of the microdomains, that is, $R_{ex,BCC} \geq R_{ex,P(q)}$, and $R'_{ex,C(PMAA)} \geq R'_{ex,P'(q)}$. Obviously, this condition is only fulfilled for the case of the SPH microdomains with BCC arrangement. So, the possibility of *C*(PMAA) morphology is rejected and we assign BCC as the morphology of the samples of S(MD)-MAA(PD)-17-M system. This is in line with the observed lack of optical anisotropy of the samples, revealed by inspecting them between crossed polarizers.

In the above mentioned analysis, we assumed that $\Phi^{Seg}_{PMAA}=\Phi_{PMAA}$, needed for calculation of $R_{ex,BCC}$ and $R'_{ex,C(PMAA)}$ from eqs 8 and 9, respectively. After assigning the morphology to be BCC, we are now in the position to remove this assumption and calculate the value of $\Delta\Phi_{PMAA}$. We have

$$\Delta\Phi_{PMAA}=1-\frac{\Phi^{Seg}_{PMAA}}{\Phi_{PMAA}}=1-\frac{4\pi n_u\int_0^\infty R^3 p(R)dR}{3\Phi_{PMAA}\alpha^3\int_0^\infty p(R)dR} \quad (11)$$

$p(R)$ being defined in eq 5 with $\overline{R}=R_{ex,P(q)}$. The acquired values of $\Delta\Phi_{PMAA}$ are shown in Figure 3.

S(MD)-MAA(PD)-30-M System

The scattering results for samples of the mixture system of S(MD)-MAA(PD)-30-M at various T are presented in Figure 7. For this Φ_{PMAA} value, there is again the *a priori* possibility that we are in the *C*(PMAA) morphology of the phase diagram. This possibility is excluded by the fact that there are peaks at relative position of $\sqrt{5}$, which is a nonallowed reflection for *C*(PMAA) morphology. The assignment of BCC symmetry also agrees with our observation that all samples were non-birefringent when viewed between crossed polarizers. (It should be mentioned that we assign the maxima in the scattering patterns at relative positions of $\sqrt{10}$ (T = 208 °C) and $\sqrt{9}$ (T = 188 °C) to be Bragg reflections, and not to be form factor oscillations, because, in the vicinity of these maxima, our attempts to fit to the scattering patterns the sphere form factor failed.)

Thus, systems of S(MD)-MAA(PD)-15, S(MD)-MAA(PD)-17-M, and S(MD)-MAA(PD)-30-M exhibit a BCC arrangement of microdomains. This is particularly interesting for S(MD)-MAA(PD)-15 and S(MD)-MAA(PD)-30-M, where, considering that sometimes it is difficult to obtain well-ordered BCC structures even in near-MD block copolymer systems, despite the molecular weight (and the architectural) polydispersity, they are microphase separated into a very well-ordered BCC structure. Presumably the near-MD characteristic of the majority component (and triblock midblock) and the high volume fraction of the PMAA material (due to the asymmetry in the phase diagram), have favored BCC arrangement of microdomains. To our knowledge, this is the first time that such a phenomenon is observed in block copolymer systems exhibiting block (and architectural) polydispersity.

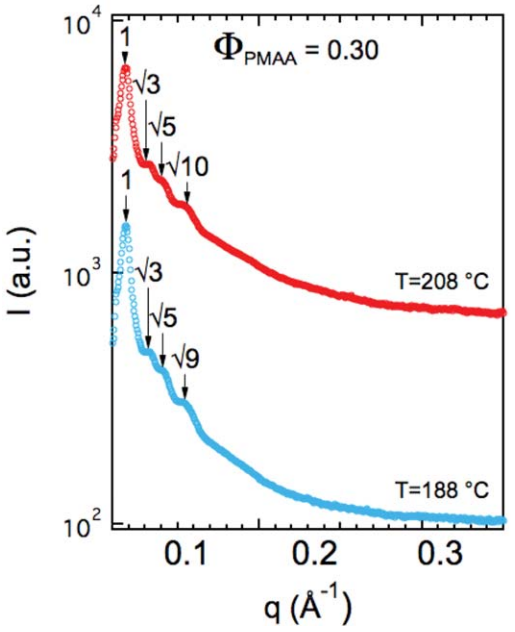

FIGURE 7 SAXS results for the mixture system of S(MD)-MAA(PD)-30-M at T = 188°C (blue) and T = 208°C (red). Observed BCC reflections are identified. All samples were non-birefringent, when viewed between crossed polarizers.

TABLE 4 Characteristics of SPH Microdomains Ordered in a BCC Arrangement for Systems of S(MD)-MAA(PD)-15 and S(MD)-MAA(PD)-30-M

System	T (°C)	α (Å)	$R_{ex,BCC}$[a] (Å)
S(MD)-MAA(PD)-15	188	535	139
	202	504	131
S(MD)-MAA(PD)-30-M	174	477	156
	188	489	160
	202	578	189
	208	501	164

[a] From eq 8 by assuming that $\Phi^{Seg}_{PMAA}=\Phi_{PMAA}$.

Effect of Polydispersity on the Microphase Separation Behavior

Interaction Parameter

For this system, no ODT has been observed up to 230 °C by rheology or SAXS, so an experimental determination of the Flory-Huggins interaction parameter χ based on weak-segregation-regime WSR calculation of χ at T_{ODT}[63] or correlation hole in disordered state[63,64] is impossible. This is frequently the case for systems in SSR.[65–67] Hence, for calculation of the phase diagrams, we will instead estimate χ from solubility parameters

$$\chi=\left(\frac{v_0}{k_BT}\right)(\delta_{PS}-\delta_{PMAA})^2 \quad (12)$$

where k_B is the Boltzmann constant, T is temperature in Kelvin and we have taken common segmental volume of v_0 = 139 Å^3. This method is valid if the conformation symmetry parameter defined as[68]

$$\beta_i^2=b_i^2\Big/_{6v_i} \quad (13)$$

is not too high for each block[69] (b_i is the statistical segment length for the i-block). This is indeed the case for our two blocks where we have β^2_{PS} = 0.0467 Å^{-1} and β^2_{PMAA} = 0.0548 Å^{-1} based on b_{PS} = 6.8 Å[70] and b_{PMAA} = 6.2 Å estimated from the radius of gyration of an unperturbed coil of PMAA.[71] For our systems, the segregation strength χZ thus calculated (based on v_0 = 139 Å^3) lies in the range $79 \le \chi Z \le 232$. If we put this beside the fact that we did not observe an ODT by SAXS or rheology up to 230 °C, we may conclude that we are essentially in the SSR (the onset of the SSR for diblock copolymer systems is approximately at χZ = 50[72]).

Phase Diagrams of S(MD)-MAA(MD) and S(MD)-MAA(MD)-S(MD)

The phase diagrams of S(MD)-MAA(MD) and S(MD)-MAA(MD)-S(MD) systems, computed using SCFT of HW[34–37] are presented in Figure 8(a,b). HW theory takes into account the stability of the following morphologies with respect to the molecularly homogenous H state: closed-packed spheres of PMAA *CPS*(PMAA), hexagonally packed cylinders of PMAA *C*(PMAA), lamellar structure *L*, hexagonally packed cylinders of PS *C*(PS) and closed-packed spheres of PS *CPS*(PS).

For S(MD)-MAA(MD) [Fig. 7(a)], in the microphase separated region of the phase diagram, it is observed that (i) upon an increase in Φ_{PMAA} a morphological sequence of *CPS*(PMAA) → *C*(PMAA) → *L* → *C*(PS) → *CPS*(PS) occurs, (ii) the boundaries between various morphologies are almost vertical with respect to the axis of Φ_{PMAA}, occurring at Φ_{PMAA} values of ≈ 0.13 [*CPS*(PMAA)/*C*(PMAA)], ≈ 0.35 [*C*(PMAA)/*L*], ≈ 0.69 [*L*/*C*(PS)], and ≈ 0.91 [*C*(PS)/*CPS*(PS)], and (iii) the phase diagram is slightly asymmetric about Φ_{PMAA}=0.50. The latter is the result of the conformational asymmetry

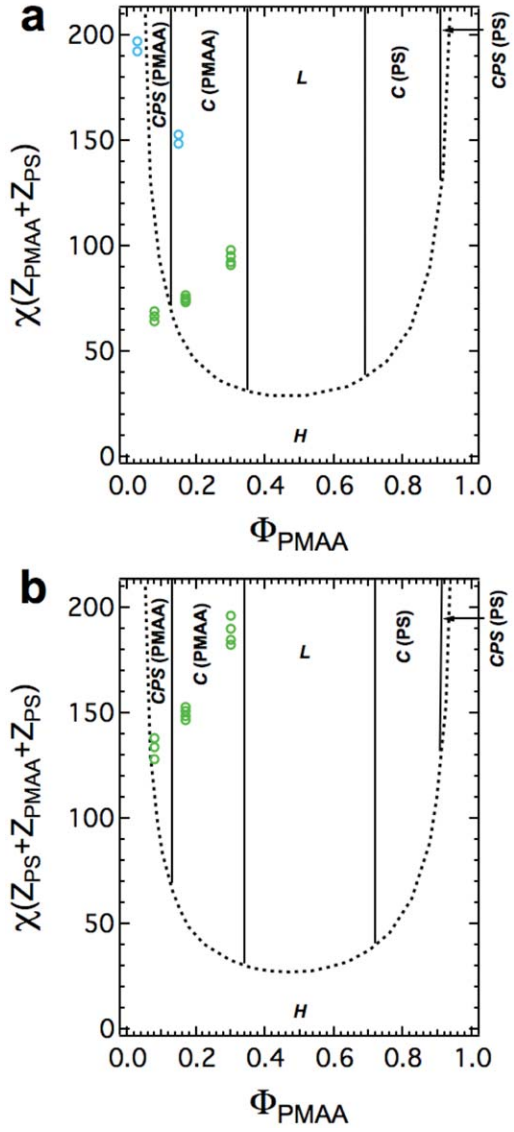

FIGURE 8 Computed phase diagrams for (a) S(MD)-MAA(MD) and (b) S(MD)-MAA(MD)-S(MD) systems by using HW theory; (blue) the hypothetical MD equivalents to the neat diblock systems and (green) the hypothetical MD equivalents of the mixture components, studied in this work.

between the two blocks that, for an A-B diblock copolymer, is quantified by a parameter ε.

$$\varepsilon = \frac{\beta_{PB}^2}{\beta_{PA}^2} \quad (14)$$

Thus, we have $\varepsilon = \frac{\beta_{PMAA}^2}{\beta_{PS}^2} = 1.17 > 1$, that conforms to the slight asymmetric nature of our calculated phase diagram.[73–75] The calculated phase diagram for S(MD)-MAA(MD)-S(MD) system [Fig. 8(b)] is very similar to the one for S(MD)-MAA(MD) system, in terms of the stability limits of (i) the microphase separated region and (ii) the various morphologies. Thus, the morphological boundaries are practically unaltered, occurring at Φ_{PMAA} values of ≈ 0.13 [CPS(PMAA)/*C*(PMAA)], ≈ 0.34 (*C*(PMAA)/*L*, ≈ 0.72 [*L*/*C*(PS)], and ≈ 0.91 (*C*(PS)/*CPS*(PS)). We are only aware of one relevant previous experimental study on the morphological investigation of S(MD)-MAA(MD) diblock copolymer.[76] In this study, it is reported that a single sample with $\Phi_{PMAA} \approx 0.14$ and $\chi Z >> 100$ exhibited *C*(PMAA) morphology, which is in agreement with what is predicted in our calculated phase diagram of S(MD)-MAA(MD) system. We are unaware of a previous experimental study on the morphological investigation of S(MD)-MAA(MD)-S(MD) triblock copolymers, so, unfortunately, we cannot compare our calculated phase diagram for S(MD)-MAA(MD)-S(MD) system with relevant experimental results.

S(MD)-MAA(PD)-%$_{PMAA}$ Diblock Systems

Let us compare microphase separation behavior of our experimental systems of S(MD)-PMAA(PD)-3 and S(MD)-PMAA(PD)-15 (studied in subsections "SPH Microdomains in Disordered Liquid-like State at Low Φ_{PMAA}" and "SPH Microdomains in Ordered Liquid Crystalline State at High Φ_{PMAA}", respectively) with the microphase separation behavior of their hypothetical MD counterparts, that is, S(MD)-PMAA(MD)-3 and S(MD)-PMAA(MD)-15, respectively, at various *T*. It is revealed that:

1. Regardless of the value of *T*, while the hypothetical S(MD)-PMAA(MD)-3 system is in *H* (disordered) state [see Fig. 8(a)] our experimental S(MD)-PMAA(PD)-3 system is (a) microphase separated, and (b) exhibits a SPH liquid-like morphology. Observation (a) is in line with the experimental[8,22] and the theoretical[10,14,15,20,21] studies, reporting that for a compositionally asymmetric diblock copolymer with a PD minority block there is a reduction in $(\chi Z)_{ODT}$. Thus, we propose that the PD nature of the minority block of our experimental S(MD)-PMAA(PD)-3 system results in stabilization of the microphase separated state versus *H* state. To our knowledge, this is the first time that the occurrence of such a phenomenon is experimentally identified when (i)′ the experimental A(MD)-B(PD) system is compositionally highly asymmetric ($\Phi_B << 0.5$), and (ii)′ the microdomain morphology is SPH. Observation (*b*) is in line with the fact that out of the total number of the PMAA blocks of the experimental S(MD)-PMAA(PD)-3 system there is a non-zero fraction $\Delta\Phi_{PMAA}$ that are dislodged from the PS/PMAA interface, because they are very short (see subsection SPH Microdomains in Disordered Liquid-Like State at Low **PHI**$_{PMAA}$ and Fig. 3). This fraction of nonmicellized chains acts as a diluent, allowing for larger fluctuations in the position of the block copolymer microdomains, which inhibits the formation of long-range order (although the micelle coronas are made of MD PS chains[11]).
2. Regardless of *T*, while the hypothetical S(MD)-PMAA(MD)-15 system has the *C*(PMAA) morphology [see Fig. 8(a)], our experimental S(MD)-PMAA(PD)-15 system consists of SPH(PMAA) microdomains in BCC arrangement. This is a direct consequence of polydispersity in the PMAA block. As it was mentioned before, polydispersity in PMAA blocks reduces entropic elasticity of PMAA microdomains, which in turn facilitates formation of an interface curved toward them.[10,11] This effect is similar to what is observed in simulations of asymmetric diblock copolymers with an MD majority block and a PD minority block.[15,24] In ref. [15], it was found that for $\Phi = 0.30$ a BCC phase is favorable over a *C* phase. However, for a chemically relevant diblock copolymer of poly(styrene)-*b*-poly(acrylic acid), with both PD PS and poly(acrylic acid) PAA blocks, that is, S(PD)-AA(PD), $(0.09 \leq \Phi_{PAA} \leq 0.84)$, it was found that for asymmetric block copolymer-based systems the morphology can be different from SPH, being *C* (for $\Phi_{PAA} = 0.23$) and a coexistence of *C* and *L* (for $\Phi_{PAA} = 0.29$).[77]
3. Regardless of the value of *T*, the SPH microdomain sizes of these two experimental systems are always higher than those of the hypothetical MD counterparts, determined using SSR theories of Nyrkova et al.[39] (NKD) and Semenov et al.[40] (SNK) (Please see Fig. 9; notice that since HW model does not predict SPH microdomain morphology for the hypothetical cases, in principle, we cannot use it for size calculations; nevertheless, regardless of *T*, assuming

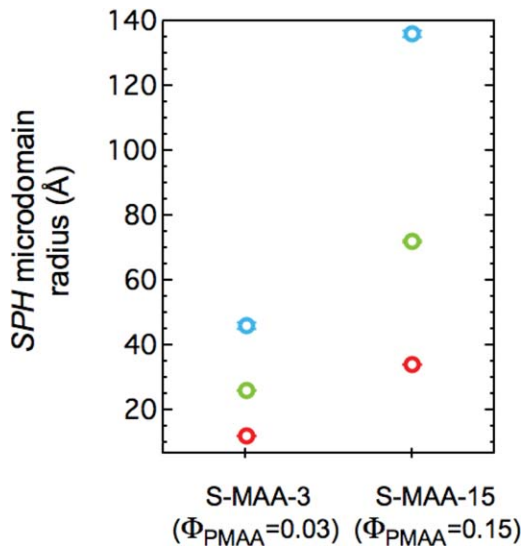

FIGURE 9 The radii of SPH microdomains of the experimental S(MD)-MAA(PD)-%$_{PMAA}$ (blue) and the theoretical S(MD)-MAA(MD)-%$_{PMAA}$, NKD (red) and SNK (green), systems with various Φ_{PMAA} values.

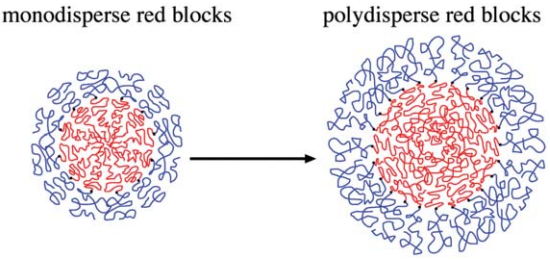

FIGURE 10 Schematics of the effect of polydispersity of the minority block on the SPH microdomain size.

that *CPS*(PMAA) is the correct morphology for these hypothetical cases, HW model gives values for the SPH microdomain sizes that are less than those of the experimental systems].

While there are several models for L[10,12,13,78,79] and C[10,80] microdomains that specifically address the question of the microdomain size increase of PD diblock copolymers relative to MD case, we are unaware of such a model for SPH microdomains. But, the physics of polydispersity-induced increase of SPH microdomain size should essentially be the same. In a PD system, shorter PMAA blocks do not extend far from the interface, allowing the longer PMAA blocks to have a less stretched conformation in the space filled further away from the interface, thus decreasing their elastic stretching free energy (Fig. 10).

In a previous study[16] on blends of the ionomeric form of diblock copolymers similar to those of our study (i.e., poly(styrene)-*b*-poly(cesium methacrylate)) it was shown that an increase in $PDI_{ionomer}$ (up to 3.1) does not affect the size of SPH(PMACs) microdomains. The authors concluded that this insensitivity to polydispersity was caused by the nonequilibrium nature of neutralization process. However, for blends of poly(styrene)-*b*-poly(4-vinylpyridinium methyl iodide) diblock copolymer an increase in $PDI_{ionomer}$ (up to 3.6) was accompanied by an increase in the SPH microdomain size. To our knowledge, this article is the first where the effect of the PD nature of the minority block on microdomain size increase of neat (nonblended) asymmetric diblock copolymers in the SSR is addressed.

S(MD)-MAA(PD)-%$_{PMAA}$-M Diblock/Triblock Mixture Systems

In our three experimental mixture systems of S(MD)-MAA(PD)-%$_{PMAA}$-M (%$_{PMAA}$ = 100 × Φ_{PMAA}, Φ_{PMAA} = 0.08, 0.17, and 0.30; whose morphologies were previously determined in subsection "SPH Microdomains in Disordered Liquid-like State at Low Φ_{PMAA}" and "SPH Microdomains in Ordered Liquid Crystalline State at High Φ_{PMAA}"), while the matrix of the PS material is composed of a single population of MD PS chains, the discrete SPH microdomains of the PMAA material are composed of two populations of PMAA chains, one belonging to the diblocks and another to the triblocks. We believe that the latter fact, in analogy with the physics of diblock copolymers comprising of PD block(s) [explained in detail in section "Introduction" and subsection "Phase diagrams of S(MD)-MAA(MD) and S(MD)-MAA(MD)-S(MD)"], induces a reduction in the entropic elasticity of PMAA domains. In light of this consideration, let us examine in more detail the microphase separation behavior of these mixtures by comparing them with the hypothetical MD equivalents to their components, that is, S(MD)-MAA(MD)-%$_{PMAA}$ and S(MD)-MAA(MD)-S(MD)-%$_{PMAA}$ (%$_{PMAA}$ = 100 × Φ_{PMAA}, Φ_{PMAA} = 0.08, 0.17, and 0.30), at various T. It is revealed that:

1. Regardless of the value of T, while the experimental mixture system of S(MD)-MAA(PD)-8-M exhibits SPH liquid-like morphology, the hypothetical system of S(MD)-MAA(MD)-8 is in H state and the hypothetical system of S(MD)-MAA(MD)-S(MD)-8 exhibits *CPS*(PMAA) morphology [see Fig. 8(a,b)].
2. Regardless of T, while the experimental mixture systems of S(MD)-MAA(PD)-17-M and S(MD)-MAA(PD)-30-M exhibit BCC morphology, all the hypothetical MD equivalents of the mixture components of these two systems have a *C*(PMAA) morphology. This observation is consistent with the anticipated reduced entropic elasticity of the PMAA microdomains, caused by the PD nature of the PMAA chains facilitating formation of an interface curved toward them.
3. We have determined the nonzero values of $\Delta\Phi_{PMAA}$ for two experimental mixture systems of S(MD)-MAA(PD)-8-M and S(MD)-MAA(PD)-17-M (see Fig. 3). We believe that the occurrence of the liquid-like morphology of the former and the poor degree of long-range order of the latter (as it is revealed through the lack of the sharp higher-order reflections of the BCC structure in the SAXS patterns of Fig. 6) is closely correlated to the nonzero nature of $\Delta\Phi_{PMAA}$. This is due to the fact that the diblock and the triblock molecules that are unanchored from the PS/PMAA interface and swell the PS matrix act as diluent and allow for larger fluctuations in the positions of the SPH microdomains (in spite of the fact that the corona of the SPH microdomains are made of MD PS chains[11]).

CONCLUSIONS

The strong segregation regime SSR microphase separation behavior of samples of compositionally (highly) asymmetric (i) two diblock copolymers and (ii) three mixtures M of diblock and triblock copolymers (the latters obtained as end-coupling products of two diblock molecules of the mixture), composed of (a) MD majority block(s) of PS and a PD minority block of PMAA, symbolized as S(MD)-MAA(PD)-%$_{PMAA}$ and S(MD)-MAA(PD)-%$_{PMAA}$-M, respectively (%$_{PMAA}$ = 100 × Φ_{PMAA}, $0.03 \leq \Phi_{PMAA} \leq 0.30$; %$_{PMAA}$ and Φ_{PMAA} denote the volume percent and the volume fraction of PMAA chains, respectively), was studied by means of rheology, crossed polarizers, WAXS (see the Supporting Information 2) and SAXS techniques, together with SAXS modeling analysis.

Samples of S(MD)-MAA(PD)-%$_{PMAA}$ and S(MD)-MAA(PD)-%$_{PMAA}$-M systems show morphologies of PMAA-filled

spherical SPH(PMAA) microdomains, dispersed in a matrix of PS material, either in disordered liquid-like state (for $0.03 \leq \Phi_{PMAA} \leq 0.08$) or body-centered-cubic BCC arrangement (for $0.15 \leq \Phi_{PMAA} \leq 0.30$), at various annealing temperatures *T*. By comparing the experimental systems of S(MD)-MAA(PD)-$\%_{PMAA}$ (Φ_{PMAA} = 0.03 and 0.15) with the hypothetical MD equivalent systems of S(MD)-MAA(MD)-$\%_{PMAA}$ (Φ_{PMAA} = 0.03 and 0.15), the effects of the polydispersity of the PMAA minority block of the formers are found to be the followings. (i) Microphase separated state is favored over an anticipated molecularly homogenous state (for $\Phi_{PMAA}=0.03$), (ii) BCC structure is favored over an anticipated hexagonally packed PMAA cylindrical *C*(PMAA) morphology (for $\Phi_{PMAA}=0.15$), (iii) a fraction of PMAA chains $\Delta\Phi_{PMAA}$, due to their very short lengths, are unanchored from the PS/PMAA interface and swell the PS matrix (for $\Phi_{PMAA}=0.03$); value of $\Delta\Phi_{PMAA}$ increases when *T* increases, and (iv) the SPH microdomains are dilated (for $\Phi_{PMAA}=0.03$ and 0.15). Similarly, for mixture systems of (MD)-MAA(PD)-$\%_{PMAA}$-M (Φ_{PMAA} = 0.08, 0.17, and 0.30) it was found that (i) $\Delta\Phi_{PMAA}$ has nonzero values (for $\Phi_{PMAA}=0.08$ and 0.17), and (ii) BCC structure is favored over the anticipated *C*(PMAA) morphology of the hypothetical MD equivalents of the mixture components, i.e. S(MD)-MAA(MD)-$\%_{PMAA}$ and S(MD)-MAA(MD)-S(MD)-$\%_{PMAA}$ (for $\Phi_{PMAA}=0.17$ and 0.30). Interestingly, in both S(MD)-MAA(PD)-$\%_{PMAA}$ and S(MD)-MAA(PD)-$\%_{PMAA}$-M systems, despite molecular weight (and architectural) polydispersity, very well-ordered BCC structures are observed. Furthermore, we point out the fact that the occurrence of a liquid-like morphology (for $\Phi_{PMAA}=0.03$ and 0.08) and a poor degree of long-range BCC order (for $\Phi_{PMAA}=0.17$) are correlated to the nonzero nature of $\Delta\Phi_{PMAA}$. Finally, there was no indication of phase separation on macroscopic and mesoscopic length scales.

ACKNOWLEDGMENTS

Financial support by the Swedish Research Council (VR) through the Linnaeus grant for the Organizing Molecular Matter (OMM) Center of Excellence (239-2009-6794) is gratefully acknowledged.

REFRENCES AND NOTES

1 I. W. Hamley, The Physics of Block Copolymers, Oxford University Press, New York, **1998**.

2 J. S. Wang, K. Matyjaszewski, *J. Am. Chem. Soc*. **1995**, *117*, 5614–5615.

3 M. Kato, M. Kamigaito, M. Sawamoto, T. Higashimura, *Macromolecules* **1995**, *28*, 1721–1723.

4 K. Matyjaszewski, *Macromol. Symp.* **2001**, *174*, 51–67.

5 J. Chiefari, Y. K. Chong, F. Ercole, J. Krstina, J. Jeffery, T. P. T. Le, R. T. A. Mayadunne, G. F. Meijs, C. L. Moad, G. Moad, E. Rizzardo, S. H. Thang, *Macromolecules* **1998**, *31*, 5559–5562.

6 G. Moad, R. T. A. Mayadunne, E. Rizzardo, M. Skidmore, S. H. Thang, *Macromol. Symp.* **2003**, *192*, 1–12.

7 N. A. Lynd, A. J. Meuler, M. A. Hillmyer, *Prog. Polym. Sci*. **2008**, *33*, 875–893.

8 A.-V. Ruzette, S. Tence-Girault, L. Leibler, F. Chauvin, D. Bertin, O. Guerret, P. Gerard, *Macromolecules* **2006**, *39*, 5804–5814.

9 N. A. Lynd, M. A. Hillmyer, *Macromolecules* **2005**, *38*, 8803–8810.

10 D. M. Cooke, A.-C. Shi, *Macromolecules* **2006**, *39*, 6661–6671.

11 M. W. Matsen, *Phys. Rev. Lett.* **2007**, *99*, 148304.

12 M. W. Matsen, *Eur. Phys. J. E* **2006**, *21*, 199–207.

13 S. T. Milner, T. A. Witten, M. E. Cates, *Macromolecules* **1989**, *22*, 853–861.

14 C. Burger, W. Ruland, A. N. Semenov, *Macromolecules* **1990**, *23*, 3339–3346.

15 S. W. Sides, G. H. Fredrickson, *J. Chem. Phys.* **2004**, *121*, 4974–4986.

16 D. Nguyen, X.-F. Zhong, C. E. Williams, A. Eisenberg, *Macromolecules* **1994**, *27*, 5173–5181.

17 Y. Matsushita, A. Noro, M. Iinuma, J. Suzuki, H. Ohtani, A. Takano, *Macromolecules* **2003**, *36*, 8074–8077.

18 A. Noro, M. Iinuma, J. Suzuki, A. Takano, Y. Matsushita, *Macromolecules* **2004**, *37*, 3804–3808.

19 A. Noro, D. Cho, A. Takano, Y. Matsushita, *Macromolecules* **2005**, *38*, 4371–4376.

20 L. Leibler, H. Benoit, *Polymer* **1981**, *22*, 195–201.

21 K. M. Hong, J. Noolandi, *Polym. Commun*. **1984**, *25*, 265–268.

22 N. A. Lynd, M. A. Hillmyer, *Macromolecules* **2007**, *40*, 8050–8055.

23 T. M. Beardsley, M. W. Matsen, *Eur. Phys. J. E* **2008**, *27*, 323–333.

24 T. M. Beardsley, M. W. Matsen, *Macromolecules* **2011**, *44*, 6209–6219.

25 J. M. Widin, A. K. Schmitt, A. L. Schmitt, K. Im, M. K. Mahanthappa, *J. Am. Chem. Soc*. **2012**, *134*, 3834–3844.

26 J. M. Widin, A. K. Schmitt, K. Im, A. L. Schmitt, M. K. Mahanthappa, *Macromolecules* **2010**, *43*, 7913–7915.

27 A. L. Schmitt, M. K. Mahanthappa, *Soft Matter* **2012**, *8*, 2294–2303.

28 G. Hadziioannou, A. Skoulios, *Macromolecules* **1982**, *15*, 267–271.

29 M. D. Gehlsen, K. Almdal, F. S. Bates, *Macromolecules* **1992**, *25*, 939–943.

30 K. Matyjaszewski, J. Xia. In Handbook of Radical Polymerization; Wiley, USA, **2003**; p 523–628.

31 L. M. Pitet, M. A. Hillmyer, *Macromolecules* **2009**, *42*, 3674–3680.

32 N. A. Lynd, M. A. Hillmyer, M. W. Matsen, *Macromolecules (Washington, DC, US)* **2008**, *41*, 4531–4533.

33 H. Walter, C. Harrats, P. Müller-Buschbaum, R. Jérome, M. Stamm, *Langmuir* **1999**, *15*, 1260–1267.

34 J. Mark, K. Ngai, W. Graessley, L. Mandelkern, E. Samulski, J. Koenig, G. Wignall. Physical Properties of Polymers, 3rd ed.; Cambridge University Press, UK, **2004**.

35 E. Helfand, Z. R. Wasserman, *Macromolecules* **1978**, *11*, 960–966.

36 E. Helfand, Z. R. Wasserman, *Macromolecules* **1980**, *13*, 994–998.

37 E. Helfand, Z. R. Wasserman, *Macromolecules* **1976**, *9*, 879–888.

38 E. Helfand, Z. R. Wasserman, *Dev. Block Copolym.* **1982**, *1*, 99–125.

39 I. A. Nyrkova, A. R. Khokhlov, M. Doi, *Macromolecules* **1993**, *26*, 3601–3610.

40 A. N. Semenov, I. A. Nyrkova, A. R. Khokhlov, *Macromolecules* **1995**, *28*, 7491–7500.

41 S. K. Varshney, Z. Gao, X. F. Zhong, A. Eisenberg, *Macromolecules* **1994**, *27*, 1076–1082.

42 G. Wang, D. Yan, *J. Appl. Polym. Sci.* **2001**, *82*, 2381–2386.

43 K. A. Davis, B. Charleux, K. Matyjaszewski, *J. Polym. Sci. Part B: Polym. Phys.* **2000**, *38*, 2274–2283.

44 J. Listak, W. Jakubowski, L. Mueller, A. Plichta, K. Matyjaszewski, M. R. Bockstaller, *Macromolecules* **2008**, *41*, 5919–5927.

45 K. Almdal. In Developments in Block Copolymer Science and Technology; Wiley, England, **2004**, p 31–69.

46 M. Lazzari, T. Kitayama, K. Hatada, O. Chiantore, *Macromolecules* **1998**, *31*, 8075–8082.

47 D. J. Kinning, E. L. Thomas, *Macromolecules* **1984**, *17*, 1712–1718.

48 D. J. Kinning, E. L. Thomas, L. J. Fetters, *J. Chem. Phys.* **1989**, *90*, 5806–5825.

49 M. Schwab, B. Stühn, *Phys. Rev. Lett.* **1996**, *76*, 924–927.

50 M. Schwab, B. Stühn, *Colloid Polym. Sci.* **1997**, *275*, 341–351.

51 L. S. Ornstein, F. Zernike, *Proc. Acad. Sci. Amsterdam* **1914**, *17*, 793–806.

52 J. K. Percus, G. Yevick, *Phys. Rev.* **1958**, *28*, 6825.

53 N. W. Ashcroft, J. Lekner, *Phys. Rev.* **1966**, *145*, 83–90.

54 E. W. Kaler, K. E. Bennett, H. T. Davis, L. E. Scriven, *J. Chem. Phys.* **1983**, *79*, 5673–5684.

55 X. Wang, E. E. Dormidontova, T. P. Lodge, *Macromolecules* **2002**, *35*, 9687–9697.

56 K. Almdal, K. A. Koppi, F. S. Bates, *Macromolecules* **1993**, *26*, 4058–4060.

57 K. A. Koppi, M. Tirrell, F. S. Bates, K. Almdal, K. Mortensen, *J. Rheol. (NY)* **1994**, *38*, 999–1027.

58 Y. R. Hong, D. H. Adamson, P. M. Chaikin, R. A. Register, *Soft Matter* **2009**, *5*, 1687–1691.

59 J. Ilavsky, P. R. Jemian, *J. Appl. Crystallogr.* **2009**, *42*, 347–353.

60 F. S. Bates, R. E. Cohen, C. V. Berney, *Macromolecules* **1982**, *15*, 589–592.

61 M. Shibayama, T. Hashimoto, H. Kawai, *Macromolecules* **1983**, *16*, 16–28.

62 A. Guinier, G. Fournet. Small-Angle Scattering of X-rays; Wiley, USA, **1955**.

63 L. Leibler, *Macromolecules* **1980**, *13*, 1602–1617.

64 F. S. Bates, M. A. Hartney, *Macromolecules* **1985**, *18*, 2478–2486.

65 J. H. Chu, P. Rangarajan, J. L. Adams, R. A. Register, *Polymer* **1995**, *36*, 1569–1575.

66 D. A. Davidock, M. A. Hillmyer, T. P. Lodge, *Macromolecules* **2003**, *36*, 4682–4685.

67 N. Politakos, E. Ntoukas, A. Avgeropoulos, V. Krikorian, B. D. Pate, E. L. Thomas, R. M. Hill, *J. Polym. Sci. Part B: Polym. Phys.* **2009**, *47*, 2419–2427.

68 A. K. Khandpur, S. Foerster, F. S. Bates, I. W. Hamley, A. J. Ryan, W. Bras, K. Almdal, K. Mortensen, *Macromolecules* **1995**, *28*, 8796–8806.

69 K. Almdal, M. A. Hillmyer, F. S. Bates, *Macromolecules* **2002**, *35*, 7685–7691.

70 D. G. H. Ballard, G. D. Wignall, J. Schelten, *Eur. Polym. J.* **1973**, *9*, 965–969.

71 J. Pleštil, Y. M. Ostanevich, V. Y. Bezzabotonov, D. Hlavatá, J. Labský, *Polymer* **1986**, *27*, 839–842.

72 M. W. Matsen, F. S. Bates, *Macromolecules* **1996**, *29*, 1091–1098.

73 M. W. Matsen, F. S. Bates, *J. Polym. Sci. Part B: Polym. Phys.* **1997**, *35*, 945–952.

74 F. S. Bates, M. F. Schulz, A. K. Khandpur, S. Förster, J. H. Rosedale, K. Almdal, K. Mortensen, *Faraday Discuss* **1994**, *98*, 7–18.

75 J. D. Vavasour, M. D. Whitmore, *Macromolecules* **1993**, *26*, 7070–7075.

76 C. Osuji, C. Y. Chao, I. Bita, C. K. Ober, E. L. Thomas, *Adv. Funct. Mater.* **2003**, *12*, 753–758.

77 D. Bendejacq, V. Ponsinet, M. Joanicot, Y. L. Loo, R. A. Register, *Macromolecules* **2002**, *35*, 6645–6649.

78 E. B. Zhulina, T. M. Birshtein, *Polymer* **1991**, *32*, 1299–1308.

79 T. M. Birshtein, Y. V. Liatskaya, E. B. Zhulina, *Polymer* **1990**, *31*, 2185–2196.

80 J. V. Lyatskaya, E. B. Zhulina, T. M. Birshtein, *Polymer* **1992**, *33*, 343–351.